Parton distributions at small x

J. Kwiecinski,* A. D. Martin, and W. J. Stirling
Department of Physics, University of Durham, DH1 3LE, England

R. G. Roberts
Rutherford Appleton Laboratory, Chilton, Didcot, OX11 0QX, England

(Received 24 July 1990)

We perform a next-to-leading-order QCD analysis of the recent data for deep-inelastic lepton-nucleon scattering and related processes, in which we pay particular attention to the forms of the parton distributions at very small x. We discuss in detail, and we incorporate in the analysis, the theoretical QCD results leading to the singular $x^{-1/2}$-type behavior of the gluon and sea-quark distributions, as well as the modifications due to shadowing effects. We find the QCD shadowing corrections are significant for $x \lesssim 10^{-3}$ even though the parton distributions are below their saturation limit. We give predictions for the structure functions F_2 and F_L accessible at the DESY ep collider HERA, and for W and Z production up to the energies of the CERN Large Hadron Collider and the Superconducting Super Collider. We discuss the possibility of experiments at these colliders probing the parton distributions in the very-small-x region.

I. INTRODUCTION

The small-x limit of parton distributions is of considerable importance both theoretically and phenomenologically. We shall be primarily concerned with deep-inelastic lepton-proton scattering for which

$$x=\frac{Q^2}{2M\nu} ,$$

where M is the proton mass, $Q^2 \equiv -q^2$, $\nu \equiv p\cdot q/M$, with q being the four-momentum transfer between the incoming and outgoing lepton and p being the proton four-momentum. We are particularly interested in the small-x region, $2M\nu \gg Q^2$, in which Q^2 is also kept large (i.e., at least a couple of GeV^2 or so), so that the QCD-improved parton model is applicable. This region of very small x and large Q^2 will soon be probed by experiments at the DESY ep collider HERA.

One of the most important predictions of perturbative QCD in this very-small-x limit is the strong increase of the gluon and sea-quark distributions.[1] This has implications far beyond deep-inelastic lepton-nucleon scattering and is, in fact, relevant to all high-energy hadron collisions. Indeed the dramatic increase of the parton distributions at small x can in many cases compensate the inherent "smallness" of the cross sections of the "hard" QCD subprocesses which contribute to a particular hadron-hadron collision. As a consequence, at sufficiently high energy these processes, which correspond to the collisions of partons carrying a very small fraction of the momentum of their parent hadron, can compete successfully with the "soft" processes which have traditionally been regarded as being responsible for the bulk of the hadronic cross section. Unlike the "soft" processes, these so-called "semihard" processes can be computed in perturbative QCD. As the energy increases the semihard processes are expected to give an increasing and an appreciable part of the total hadronic cross section.[2]

The measurements of the structure functions of deep-inelastic lepton-nucleon scattering that have so far been performed do not reach into the small-x regime for $Q^2 \gtrsim 4$ GeV^2.[3-7] On the other hand, many detailed theoretical QCD studies have been made to predict the general form of the parton distributions at small x.[1,8] Clearly these theoretical expectations must be incorporated in any phenomenological analysis of structure-function data which hopes to give realistic extrapolations of the parton distributions into the experimentally unexplored and important small-x regime.

The traditional double leading-logarithm [$\ln(Q^2)$ and $\ln(1/x)$] approximation is not appropriate for the form of the gluon and sea-quark distributions at very small x. An alternative summation of QCD diagrams is necessary giving a small-x behavior of these distributions which may be approximated by

$$xf_i(x,Q^2) \sim h_i(Q^2)x^{-\lambda} ,$$

with $\lambda \sim 0.5$. In Sec. II we attempt to expose, in the simplest possible way, the physical ideas that underlie this theoretical prediction.

The very strong growth in the number of partons with decreasing x leads in turn to another problem which must be addressed. As we have mentioned above, as x decreases an increasing number of partons could initiate the semihard process and, though the cross section for any individual subprocess is relatively small, the total interaction area eventually becomes comparable to the area of the proton: the partons then spatially overlap and can no longer be regarded as free. Their interaction leads to shadowing effects which can eventually result in parton saturation. The indefinite increase of parton distributions

with decreasing x is thereby slowed down; yet they exhibit linear scaling violation. These shadowing effects are, in principle, reasonably well understood theoretically, and clearly must be incorporated if the results of a phenomenological analysis are extrapolated to very small x. Again we attempt, in Sec. III, a simple review of the underlying theoretical ideas in preparation for the phenomenological study which we present in Sec. IV.

The experimental data at present available for $Q^2 \gtrsim 4$ GeV^2 lie in an x range ($x \gtrsim 0.01$) for which the singular $x^{-1/2}$ behavior and the shadowing corrections are not important. In other words, in a purely phenomenological analysis the shapes of the parton distributions are still to a large extent determined by terms which are nonleading in the small-x limit. As we have emphasized above, if we wish to extrapolate the results of such a structure-function analysis into the very-small-x region we must choose parametric forms of the "starting" parton distributions at $Q^2=Q_0^2$ ($=4$ GeV^2) which can accommodate the theoretical expectations at small x. The parametric forms that we fit to the available data are given in Sec. IV, and incorporate the theoretical expectations at small x that we discuss in Sec. II. It is in this latter respect that the phenomenological analysis, presented here, differs from our previous work,[9] hereafter referred to as HMRS. In Sec. IV we present the new "global" fit to the deep-inelastic and related data, and show some of the properties of the resulting parton distributions.

When the parton distributions are extrapolated to make predictions in the small-x region, below that of the existing data, we include the shadowing corrections described in Sec. III. The quantitative estimate of the shadowing contributions is subject to several ambiguities, the most important one being the value of the radius parameter R describing the transverse size of the region of the nucleon where the interacting partons are concentrated. We show predictions for two different values of R which should more than span the physically acceptable range of possible values.

In Sec. V we show that the size of the sea-quark distribution at small x can be determined from the magnitude of the gluon distribution. Furthermore, the results of the phenomenological analysis, which we present in Sec. IV, turn out to be in remarkable agreement with these theoretical estimates.

One of the main objectives of extracting parton distributions from a "global" fit of deep-inelastic and related data is to provide a range of predictions at small x which incorporate *both* the singular small-x behavior *and* the shadowing corrections. We find that the shadowing effects become increasingly significant as x is extrapolated below about 10^{-3}. In Sec. VI we give predictions for the deep-inelastic electron-proton scattering structure functions F_2 and F_L in the small-x kinematic region which will be explored at HERA. Measurements of these structure functions at HERA will probe the small-x behavior of the sea-quark and gluon distributions, respectively. We also present predictions for W and Z production at the planned pp colliders which should probe the sea-quark distributions at ultrasmall x. We present our conclusions in Sec. VII.

II. THEORETICAL EXPECTATIONS FOR THE PARTON DISTRIBUTIONS AT SMALL x

It is conventional to determine the form of the parton distributions $f_i(x,Q^2)$ as functions of x and Q^2 using the Altarelli-Parisi equations, which take account of the leading (and usually the next-to-leading) powers of $\ln(Q^2)$. Starting distributions are assumed at some scale Q_0 of the order of a few GeV and the Altarelli-Parisi evolution equations are then employed to determine the distributions at higher values of Q^2. For example, for the gluon it is traditional to assume

$$xg(x,Q_0^2) \sim x^{\delta}(1-x)^{\eta} \tag{1}$$

with δ set to zero, with a similar form for the sea quarks. The small-x behavior of the parton distributions is controlled by the intercept α of the appropriate Regge-exchange trajectories

$$f_i(x,Q^2) \propto \nu^{\alpha} \propto x^{-\alpha} . \tag{2}$$

The choice $\delta=0$ in (1) for the gluon (and for the sea quarks) was originally motivated by the belief that the Pomeron describing diffractive scattering had intercept $\alpha_P=1$. However, this traditional form, with

$$xg(x,Q_0^2) \to \text{const} \quad \text{as } x \to 0 , \tag{3}$$

is not stable. When evolved to higher Q^2 it rapidly develops a steeper shape. In fact at high Q^2 we find $xg(x,Q^2)$ increases, as $x \to 0$, faster than any power of $\ln(1/x)$, but slower than any power of x. Indeed starting from a non-singular $xg(x,Q_0^2)$ it is possible to solve the Altarelli-Parisi equations analytically at very small x and large Q^2 to give

$$xg(x,Q^2) \sim \exp\{2[\xi(Q^2)\ln(1/x)]^{1/2}\} \tag{4}$$

with

$$\xi(Q^2) = \int_{Q_0^2}^{Q^2} \frac{dq^2}{q^2} \frac{C_A \alpha_s(q^2)}{\pi} , \tag{5}$$

where $C_A = N_c = 3$, the number of colors, and where we have neglected in (4) slowly varying functions of the argument of the exponential. Another manifestation of the lack of stability of the Q^2 dependence resulting from (1) is that "downwards" evolution into the region $Q^2 < Q_0^2$ would result in a distribution which became negative. This is to be contrasted with the stability in Q^2 of the small-x behavior of the valence-quark distributions

$$q_v(x,Q^2) \propto x^{-\alpha_R} , \tag{6}$$

where the intercepts $\alpha_R \sim \frac{1}{2}$ for the leading Regge trajectories responsible for nondiffractive scattering [see (27) below].

Equation (4) is known as the double leading-logarithm approximation (DLLA) as it sums the leading powers of $\ln(Q^2)$ and $\ln(1/x)$. That is, for each additional factor of α_s we keep only the $\ln(Q^2)\ln(1/x)$ term accompanying that α_s. It is useful to give a simple diagrammatic explanation of the DLLA. In axial gauges, it can be shown[10] that these leading double logarithms at large Q^2

and small x are generated by the diagrams of Fig. 1(a) in which the gluons have strongly ordered transverse momenta

$$Q^2 \gg k_T^2 \gg k_{nT}^2 \gg \cdots \gg k_{2T}^2 \gg k_{1T}^2 \gg Q_0^2 \ . \tag{7}$$

Of course the longitudinal momenta are also ordered,

$$x < x_n < \cdots < x_2 < x_1 \tag{8}$$

and, as we explain below, in the DLLA they too become *strongly* ordered. Thus as we proceed along the chain from the proton momentum p towards that of the probe q, the proton is split into smaller and smaller pieces. In each cell the integration over the transverse momentum is logarithmic (dk_{iT}^2/k_{iT}^2) and the strong ordering generates a $\ln^n(Q^2)/n!$ behavior, where the $n!$ arises from the nested form of the integrals. The integrations over the longitudinal momenta are dominated by the region in which the x_i are also strongly ordered, for which $z_i = x_i/x_{i-1}$ are small and the gluon splitting functions $P_{gg}(z_i) \sim 1/z_i$. The nested dz_i/z_i logarithmic integrations thus generate a $\ln^n(1/x)/n!$ behavior. Thus we say that the DLLA is generated by the sum of gluon ladder diagrams with strongly ordered transverse and longitudinal momenta, Fig. 1(b). The contributions in the other regions of phase space [that is, other than given by (7)] together with the contributions from nonladder diagrams are found to be nonleading. To see how the DLLA of (4) follows from the sum of ladder diagrams we simply use the relation

$$\sum_n \frac{(\frac{1}{4}y^2)^n}{(n!)^2} = I_0(y) \sim \frac{e^y}{\sqrt{2\pi y}} \tag{9}$$

for large y, where $\frac{1}{4}y^2 = \alpha_s \ln(Q^2)\ln(1/x)$ and I_0 is a modified Bessel function. If we include the running of the coupling α_s then $\alpha_s \ln(Q^2)$ becomes $\xi(Q^2) \propto \ln[\ln(Q^2)]$ of (5).

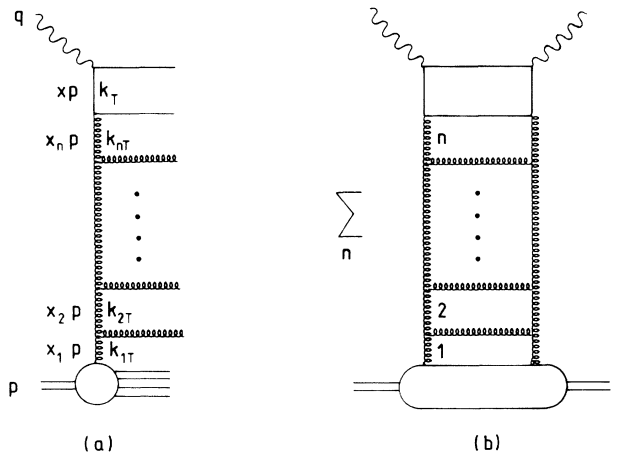

FIG. 1. Diagrammatic representation for probing the gluon content of the proton at high Q^2, where $Q^2 \equiv -q^2$. In the DLLA the transverse (k_{iT}) and longitudinal ($x_i p$) components of the gluon momenta are strongly ordered along the chain. On squaring the amplitude of (a) we generate the ladder diagram of (b) which, when summed, gives the probability of finding a gluon (k_{nT}, x_n) via a quark (k_T, x).

We now return to the lack of stability in Q^2 of (3). It hints that the gluon needs modification at very small x. Evolution using the Altarelli-Parisi equations in DLLA of a form satisfying (3) does not take into account all the leading terms in the small-x limit. It neglects, by definition, those terms in the perturbative expansion which contain the leading power of $\ln(1/x)$ but which are not accompanied by the leading power of $\ln(Q^2)$. Let us define the sum of the leading powers of $\ln(1/x)$ [and arbitrary powers of $\ln(Q^2)$] as the LL($1/x$) approximation. Thus at very small x we must, following Lipatov *et al.*,[11] sum different contributions to those of the conventional approach. We must sum LL($1/x$) terms but retain the exact Q^2 dependence, and not just LL(Q^2) terms. (Of course the gluon obtained will approach the conventional gluon at sufficiently large Q^2.) Clearly we must relax the strong ordering (7) of the k_T's, which generated the $\ln^n(Q^2)/n!$ behavior, and integrate over the full k_T phase space.

The simplest way to see the form of the small-x behavior resulting from the LL($1/x$) summation is to relate the contribution, $T_n(x, k_T^2)$, of the ladder diagram with n rungs to that with $n-1$ rungs. Here x and k_T are the longitudinal and transverse momenta of the probed gluon. In the LL($1/x$) approximation the recursion relation has the general form

$$T_n(x, k_T^2) = \int_x^1 \frac{dx'}{x'} \int dk_T'^2 K(k_T, k_T') T_{n-1}(x', k_T'^2) \ , \tag{10}$$

where the kernel K, which contains a factor of α_s, describes the emission of real gluons as well as allowing for the possibility of including virtual corrections. Depending on the form of the kernel, this relation holds whether or not the transverse momenta are ordered. For example in the DLLA the kernel is particularly simple:

$$K(k_T, k_T') = \frac{3\alpha_s}{\pi k_T'^2} \theta(k_T^2 - k_T'^2) \ , \tag{11}$$

where the θ function reflects the ordering in transverse momenta along the chain. For this kernel the recursion relation (10) has the form

$$T_n \sim \frac{3\alpha_s}{\pi} \left[\frac{1}{n} \ln \left[\frac{1}{x} \right] \right] \left[\frac{1}{n} \ln(k_T^2) \right] T_{n-1} \ , \tag{12}$$

and hence we reproduce the small-x limit (4) of the Altarelli-Parisi equation [cf. Eq. (9)].

We are, however, now interested in the case when the transverse momenta are no longer ordered. The kernel is then[11]

$$K(k_T, k_T') = \frac{3\alpha_s}{\pi} k_T^2 \left[\frac{1}{k_T'^2 |k_T^2 - k_T'^2|} - \beta(k_T^2) \delta(k_T^2 - k_T'^2) \right] \ , \tag{13}$$

where

$$\beta(k_T^2)=\int \frac{dk_T'^2}{k_T'^2}\left[\frac{1}{|k_T^2-k_T'^2|}-\frac{1}{(4k_T'^4+k_T^4)^{1/2}}\right] . \quad (14)$$

The first term in (13) corresponds to diagrams with only real gluon emission, whereas the second allows for diagrams with virtual corrections. The apparent singularity at $k_T^2=k_T'^2$ cancels between the real and virtual contributions to the kernel. Insertion of this kernel into (10) gives rise to the Lipatov equation.[11]

It is useful to first consider a simplified model in which the kernel K has a factorized form

$$K(k_T,k_T')=u(k_T)v(k_T') , \quad (15)$$

although, of course, we see that the Lipatov kernel (13) has a more complicated structure. Substitution into (10) gives

$$T_n(x,k_T^2)=u(k_T)\int_x^1 \frac{dx'}{x'}\int dk_T'^2 v(k_T')T_{n-1}(x',k_T'^2) , \quad (16)$$

which itself is of factorizable form

$$T_n(x,k_T^2)=u(k_T)t_n(x) . \quad (17)$$

Rewriting the recursion relation (16) in terms of t_n we obtain

$$t_n(x)=\lambda\int_x^1 \frac{dx'}{x'}t_{n-1}(x') , \quad (18)$$

where

$$\lambda=\int_0^\infty dk_T^2 u(k_T)v(k_T) . \quad (19)$$

Equation (18) is readily solved; the nested integrations give

$$t_n(x)\sim\frac{1}{n!}\ln^n\left[\frac{1}{x}\right]\lambda^n , \quad (20)$$

where the absence of a second $1/n!$ factor, accompanying λ^n, reflects the lack of ordering in k_T. Summing the t_n over n we thus generate the small-x behavior

$$xg(x,Q^2)\sim h(Q^2)e^{\lambda\ln(1/x)}=h(Q^2)x^{-\lambda} , \quad (21)$$

where the exponent λ, defined by (19), can be shown to be the eigenvalue of the kernel, viz.,

$$K\otimes u=\int u(k_T)v(k_T')u(k_T')dk_T'^2=\lambda u . \quad (22)$$

In general a nonfactorizable kernel, such as (13), will generate a small-x behavior given by a superposition of terms such as (21) corresponding to the various eigenvalues of the kernel. The LL$(1/x)$ behavior is given by the maximum eigenvalue, which for the Lipatov kernel of (13) can be shown to be[11]

$$\lambda_{\max}=\frac{3\alpha_s}{\pi}4\ln 2 , \quad (23)$$

and so

$$xg(x,Q^2)\sim h(Q^2)x^{-\lambda_{\max}} \quad (24)$$

as $x\to 0$. We have neglected a relatively unimportant factor of $[\ln(1/x)]^{-1/2}$ as well as terms down by powers of $\ln(1/x)$, which reflect the fact that the eigenvalue spectrum is continuous if we assume the coupling α_s is fixed. For a running coupling α_s the spectrum is discrete and the maximum eigenvalue can be shown[12] to satisfy the inequalities

$$\frac{3.6}{\pi}\alpha_s(k_0^2)\le\lambda_{\max}\le\frac{12\ln 2}{\pi}\alpha_s(k_0^2) , \quad (25)$$

where k_0^2 is the infrared cutoff applied to the integrals over the transverse momenta. Taking $\alpha_s\sim 0.25$ we have $\lambda_{\max}\sim 0.5$, which is significantly greater than zero and implies

$$xg(x,Q^2)\sim h(Q^2)x^{-1/2} \quad (26)$$

for very small x. There is nothing sacred about the precise value of the exponent $-\frac{1}{2}$; rather, Eq. (26) should be regarded as an approximate solution of the Lipatov equation. However, the singular form (26) differs appreciably from the traditional "constant" behavior assumed in (3), and moreover manifests a stability to evolution in Q^2 that was lacking in (3). Indeed a phenomenologically acceptable way to proceed is to incorporate the LL$(1/x)$ behavior of (26) in the "starting" x distribution chosen at some fixed scale $Q^2=Q_0^2$ and then to evolve according to the Altarelli-Parisi equations. This procedure, based on a form such as (26), applies equally well to the sea-quark distributions, which are driven by the gluon.

We can now understand the stability as a function of Q^2 of the leading small-x behavior of the valence-quark distributions

$$xq_v\sim x^{\delta_v}h_v(Q^2) \quad (27)$$

that we noted in (6). If $\delta_v<1$ in the input valence-quark distributions then they are more singular than the small-z behavior of the quark splitting function $P_{qq}(z)\sim$ const, and so evolution does not modify the behavior. The same is true for the gluon, but here it only applies if the exponent δ in (1) satisfies $\delta<0$ since $P_{gg}(z)\sim 1/z$ for small z.

Comparison of (26) with the Regge form of (2) shows that the Pomeron has the intercept

$$\alpha_P^0=1+\lambda_{\max}\sim 1.5 , \quad (28)$$

which is to be contrasted with the original expectation of $\alpha_P^0=1$ (or at most $\alpha_P^0=1+\epsilon$ with $\epsilon\sim 0.07$ to account for the rise of the hadronic total cross section). This implies a power growth of the QCD so-called semihard processes, which therefore become an increasing fraction of the total cross section as the energy is increased. Of course a Pomeron with intercept $\alpha_P^0>1$ will ultimately violate the Froissart bound at sufficiently high energies. It should therefore be regarded as the bare Pomeron subject to the usual unitarity corrections; hence the superscript on α_P^0.

III. SHADOWING EFFECTS AT SMALL x

We see from (21) that $xg(x,Q^2)$ grows rapidly with increasing $\ln(1/x)$ at fixed Q^2. But this increase, as x decreases, cannot go on indefinitely. If the density of gluons becomes too large they can no longer be treated as free partons. As we proceed to very small x we expect annihilation or recombination of gluons to occur and to compete with evolution so as to limit the growth of $xg(x,Q^2)$. A simple geometrical argument can be used to tell us when these gluon-gluon interactions must become significant.[1]

Consider the gluon distribution $g(x,Q^2)$ at small x in the frame in which the proton momentum p is large, but in which $xp \gg Q$. A measurement of $g(x,Q^2)$ probes a gluon of transverse size $\sim 1/Q$, but much smaller longitudinal size $\sim 1/px$. The number of gluons n_g per unit of rapidity which can interact with the probe is $xg(x,Q^2)$, since $dx = x\,dy$. Therefore the transverse area of the "thin" disc that they occupy is $\sim xg(x,Q^2)/Q^2$. When, with decreasing x, this area exceeds πR^2 (where R is the proton radius) the gluons must begin to spatially overlap in the thin disc. If we note that the gluon-gluon cross section $\hat{\sigma} \sim \alpha_s(Q^2)/Q^2$, then clearly the crucial parameter is[1]

$$W = \frac{n_g \hat{\sigma}}{\pi R^2} \sim \frac{\alpha_s(Q^2)}{\pi R^2 Q^2} xg(x,Q^2) \ . \tag{29}$$

In the region of x and Q^2 where $W \ll 1$, the interaction of gluons (in different cascade ladders) is negligible and we may continue to evolve the gluon distribution as described in Sec. II. However, at sufficiently small x, when $W \lesssim \alpha_s$, two gluons in different cascades may interact, generally fusing the gluon ladders together and decreasing the gluon density. These "shadowing" effects can be calculated[8,13,14] in perturbative QCD. To be more precise they modify the QCD evolution equation for the gluon distribution through

$$Q^2 \frac{\partial(xg(x,Q^2))}{\partial Q^2} = P_{gg} \otimes g + P_{gq} \otimes q - \frac{81\alpha_s^2(Q^2)}{16R^2Q^2} \theta(x_0 - x) \times \int_x^{x_0} \frac{dx'}{x'} [x'g(x',Q^2)]^2 \ , \tag{30}$$

where the additional nonlinear term[8] arises from the diagram shown in Fig. 2. Here we have introduced a parameter x_0 which is chosen to be sufficiently large ($\sim 10^{-2}$) so that for $x \geq x_0$ the shadowing correction is negligible. Of course the additional term will lead to a very small violation of the momentum sum rule, which we restore by a simple rescaling of the gluon distribution. The "minus" sign in the shadowing term occurs because the scattering amplitude corresponding to the gluon ladder is predominantly imaginary. It has the same physical origin as the negative contribution of the Glauber[15] double scattering term in a multiple-scattering expansion in which the single-scattering amplitude is predominantly imaginary.

The radius parameter R in the nonlinear term of (30) arises from the integration over the four-momentum k flowing along the gluon ladders in Fig. 2. Specifically R comes from the integration over the transverse components of k,

$$\frac{1}{R^2} \sim \int dk_T^2 [F(-k_T^2)]^2 \ , \tag{31}$$

and its value depends on exactly how the gluon ladders

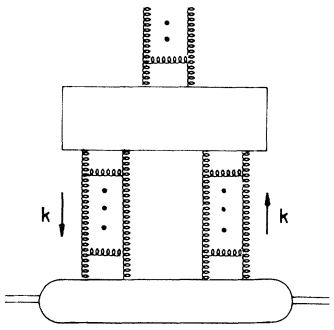

FIG. 2. Diagrammatic representation of the quadratic shadowing term in the evolution equation (30). The box represents all possible perturbative QCD diagrams which couple 4 gluons to 2 gluons; an example of one such contribution is shown in Fig. 3. The lower elongated blob represents the coupling of the proton to the gluon ladders; the two possibilities for this coupling are shown in Fig. 4.

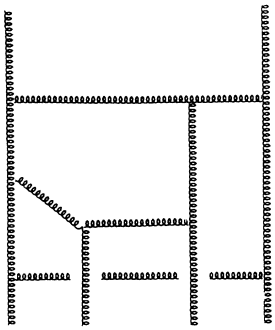

FIG. 3. An example of a QCD diagram coupling 4 gluons to 2 gluons.

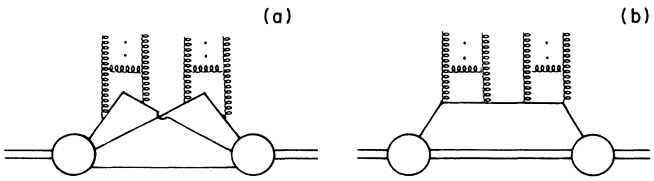

FIG. 4. Two possibilities for the coupling of the proton to the gluon ladders which is required in the shadowing diagram of Fig. 2. In (a) the ladders arise from distinct constituents of the proton, and in (b) from the same constituent.

couple to the proton. If, as is generally assumed, the ladders couple to different partons [see Fig. 4(a)], then the form factor F is characterized by the proton radius, that is, $R \sim 5$ GeV^{-1}. It has, however, been argued[8,16,17] that we should include the possibility that the ladders couple to the same constituent of the proton [Fig. 4(b)] and then it is appropriate to take R to be the radius of a valence quark, that is, $R \sim 2$ GeV^{-1}. The evolution equation (30), with $1/R^2$ factored out of the shadowing term, is of course a simplification of the actual situation. It neglects the possibility that the transverse size of the gluonic cloud of the proton increases with decreasing x.[18]

We note that the effect of the nonlinear term will be greatest for low x and low Q^2. In fact estimates[8,19] of the shadowing correction based on traditional gluon distributions, satisfying the constant small-x behavior of (3), have shown the effects are very small for $x > 10^{-4}$—less than 10% or so even for $Q^2 \sim 5$ GeV.[2] Clearly the shadowing contributions will be enhanced for the more singular and more theoretically acceptable gluon distributions satisfying (21). Indeed shadowing could be appreciable for the experiments to be performed at the DESY ep collider HERA, the CERN Large Hadron Collider (LHC), and the Superconducting Super Collider (SSC).

To study the possible importance of shadowing we base our starting gluon distribution $g(x,Q_0^2)$ on the numerical solutions of the evolution equation (30) presented in Ref. 20. We proceed as follows. We begin with the unshadowed gluon distribution $g^u(x,Q^2)$ obtained in the global analysis of the available structure function and related data, which exist only for $x > 10^{-2}$. We take the "starting" distribution to have the theoretically motivated singular form

$$xg^u(x,Q_0^2) \simeq C(x)x^{-1/2} , \tag{32}$$

where $C(x) \to$ const for very small x [see (21)]. We then impose shadowing corrections by modifying $g^u(x,Q_0^2)$ for $x < x_0$ $(=10^{-2})$ through

$$xg(x,Q_0^2) = xg^u(x,Q_0^2)\{1+\theta(x_0-x)[C(x)x^{-1/2}-C(x_0)x_0^{-1/2}]/xg_{\rm sat}(x,Q_0^2)\}^{-1} . \tag{33}$$

The distribution $xg_{\rm sat}$ is defined to be the gluon distribution which makes the right-hand side of the evolution equation (30) identically zero in the DLLA at very small x. That is,

$$\frac{3\alpha_s}{\pi}xg_{\rm sat} = \frac{81\alpha_s^2}{16R^2Q^2}(xg_{\rm sat})^2 ,$$

which gives

$$xg_{\rm sat}(x,Q^2) = \frac{16R^2Q^2}{27\pi\alpha_s(Q^2)} . \tag{34}$$

In the leading shadowing approximation $g_{\rm sat}$ is the value of the gluon which would saturate the unitarity limit. Of course, if we were to proceed to ultrasmall x, higher-order shadowing contributions would become significant and would need to be included in the evolution equation. Eventually we would pass from the region in which $W \sim \alpha_s$ into the region where $W \sim 1$, that is, the region where the saturation limit is reached [see (29) and (34)]. In the $W \sim 1$ region we have to sum over an infinite number of shadowing contributions. A possible way of performing this summation has been presented by Mueller.[21]

The phenomenological starting distribution of the gluon given by (33) has some nice features. First, xg becomes equal to the unshadowed form xg^u when shadowing is unimportant, that is, when $R \to \infty$ and $xg_{\rm sat} \to \infty$. Second, from (33) we see that $xg \to xg_{\rm sat}$ when $x \to 0$ and moreover that xg joins smoothly onto the unshadowed form xg^u at $x = x_0$ $(=10^{-2})$. Finally, the analytical form (33) reproduces to high accuracy the numerical solution of (30) that was obtained in Ref. 20.

Given the starting distribution of the gluon at $Q^2 = Q_0^2$ we evolve to higher Q^2 using (30), but of course taking into account the next-to-leading-order contributions in the first two terms which are shown symbolically on the right-hand side of the equation. Shadowing effects thus enter our phenomenological study (i) in the modification of the starting distribution in the small-x region, $x < x_0$, and (ii) by the inclusion of the nonlinear term in the evolution equation (30).

The shadowing corrections to the gluon distribution are also reflected in the sea-quark distributions $q_s(x,Q^2)$ which at small x are predominantly driven by the gluon. These corrections will, in turn, modify our predictions for the structure function $F_2^{ep}(x,Q^2)$. We assume our starting value Q_0^2 of Q^2 is large enough that the gluon-sea driving relation is established and so we modify the sea-quark "starting" distribution in the region $x < x_0$ in pro-

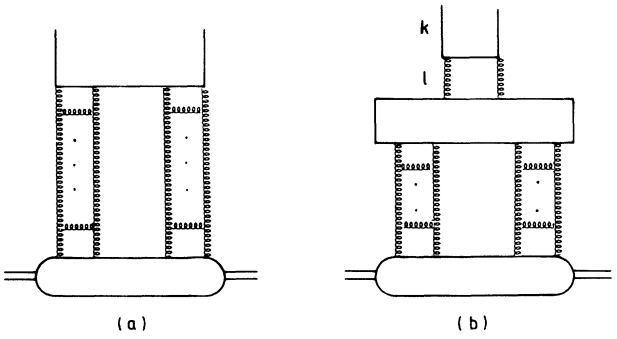

FIG. 5. Diagrams giving rise to shadowing corrections to the evolution equation, (36), for the sea-quark distributions.

portion to the shadowing correction to the gluon, that is,

$$xq_s(x,Q_0^2)=xq_s^u(x,Q_0^2)\frac{g(x,Q_0^2)}{g^u(x,Q_0^2)}\ , \tag{35}$$

where, as before, the superscript u denotes the unshadowed distribution. We tested the reliability of (35) in the extreme case of supposing that the sea-quark distributions are entirely radiatively generated[22] from the valence quarks and a valencelike gluon distribution at $Q^2=0.2$ GeV^2. Using this radical assumption we evolve with and without the nonlinear shadowing terms in (30) and find that (35) is satisfied to better than an accuracy of 10% even by $Q^2=4$ GeV^2.

There are also shadowing corrections to the evolution equation for the sea-quark distributions. The leading contributions correspond to the diagrams of Fig. 5 and the evolution equation becomes[8]

$$Q^2\frac{\partial(xq_s(x,Q^2))}{\partial Q^2}=P_{qg}\otimes g+P_{qq}\otimes q_s-\frac{27\alpha_s^2(Q^2)}{160R^2Q^2}[xg(x,Q^2)]^2+\frac{\alpha_s(Q^2)}{\pi Q^2}\theta(x_0-x)\int_x^{x_0}\frac{dx'}{x'}\frac{x}{x'}\gamma(x/x')x'G_H(x',Q^2), \tag{36}$$

where $\gamma(y)=-2y+15y^2-30y^3+18y^4$ and G_H satisfies

$$Q^2\frac{\partial(xG_H(x,Q^2))}{\partial Q^2}=-\frac{81\alpha_s^2(Q^2)}{16R^2}\theta(x_0-x)\int_x^{x_0}\frac{dx'}{x'}[x'g(x',Q^2)]^2\ . \tag{37}$$

The penultimate term in (36) arises from Fig. 5(a); in comparison to the last term of (30) the logarithmic integration over dx'/x' is absent, essentially because the $4g\to q\bar{q}$ splitting function is less singular than the $4g\to 2g$ splitting function. The last term of (36) arises from the diagram shown in Fig. 5(b). The strongly ordered part of this contribution (corresponding to $k_T^2\gg l_T^2$) has already been included, leading to the usual logarithmic integration dk_T^2/k_T^2 in the evolution of the gluon. However, this neglects contributions from terms that are linear in l_T^2/k_T^2, and the last term in (36) corresponds to taking $(l_T^2/k_T^2)dk_T^2/k_T^2$ in the place of the usual dk_T^2/k_T^2 contribution. We see a close similarity between (37) and the shadowing contribution to the gluon evolution equation (30). This reflects the fact that both shadowing terms originate from similar diagrams, Fig. 5(b) and Fig. 2, respectively. The only difference is the occurrence of a gluon ladder above the box in Fig. 2 which is generated by the linear $P_{gg}\otimes g$ term in (30). No such term occurs in (36).

IV. PHENOMENOLOGICAL ANALYSIS

In this section we attempt to quantify the expectations for the gluon and quark distributions at small x based on the theoretical arguments of Secs. II and III. At HERA we believe the important region opened up to new physics is the small-x region—perhaps even down to a few $\times 10^{-4}$ at low Q^2 values. Our aim, therefore, is to produce distributions which are constrained as tightly as possible by present data and which are consistent with the correct theoretical behavior as $x\to 0$ and then to examine what aspects of this behavior can be probed in the future—in particular at HERA.

As in our previous works,[9,23] we decide on a parametrization of the parton distributions at $Q_0^2=4$ GeV^2 and evolve up in Q^2, including next-to-leading-order corrections, to compute the structure functions or physical cross sections. As before we work in the modified minimal-subtraction ($\overline{\text{MS}}$) scheme. In comparing with experimental structure functions we chose to fit to the BCDMS[5] values of $F_2^{\mu p}$ rather than the EMC[4] values only because the former are actually more precisely determined at small x where we are concentrating our study. Actually after an overall renormalization of the two sets of measurements (BCDMS by -2%, EMC by $+8\%$), which is necessary to bring them in line with the recent reanalysis[24] of the SLAC data, the two data sets are mutually consistent for $x\lesssim 0.3$. As well as using the recent high-statistics deep-inelastic data for $F_2^{\mu p}$,[5] $F_2^{\mu n}/F_2^{\mu p}$,[25–27] $F_2^{\nu N}$, and $xF_3^{\nu N}$,[6] we also constrain the parton distributions by recent data on hadronic prompt photon production[28] and hadronic dimuon production.[29]

We begin by specifying the parametrization of the gluon distribution at $Q_0^2=4$ GeV^2. From the discussion in Sec. II we expect that the gluon distribution can be accommodated by the form

$$xg(x,Q_0^2)=A_g x^{-1/2}(1+\gamma_g x)(1-x)^{\eta_g}\ , \tag{38}$$

and it is the $pp\to\gamma X$ prompt-photon data of WA70 which essentially constrain the parameters γ_g and η_g. We find $\gamma_g=20$, $\eta_g=5.5$, $A_g=0.265$ gives an excellent fit. For this choice of gluon we take the sea-quark distribution at $Q_0^2=4$ GeV^2 to be

$$\begin{aligned}xS&\equiv 2x(\bar{u}+\bar{d}+\bar{s})\\&=A_s x^{-1/2}(1+\epsilon_s x^{1/2}+\gamma_s x)(1-x)^{\eta_s}\ ,\end{aligned} \tag{39}$$

since both the gluon and the sea quarks are expected to have the same leading $x\to 0$ behavior. As in Refs. 9 and 23 we generate the charm distribution through the evolution equations assuming that $c(x,Q_0^2)=0$ and that the charm quark is massless. Since we chose to fit to the BCDMS data ($\times 0.98$) we label the "singular" parame-

trizations of (38) and (39) as our B_- fit, in analogy with the E_+, E_- fits of Ref. 20. We choose a sea where, at $Q_0^2=4$ GeV^2, $\bar{u}=\bar{d}=2\bar{s}$ and find

$$A_s=0.0168, \quad \eta_s=9.9, \quad \epsilon_s=27.4, \quad \gamma_s=263 .$$

It, together with the valence quarks of (40), gives an excellent description of the Drell-Yan data of the E605 experiment when the K' factor of Ref. 9 is 1.17. For completeness we write down the values of the remaining parameters of the B_- fit; $\Lambda_{\overline{\rm MS}}^{(n_f=4)}=0.19$ GeV and the valence-quark distributions at $Q_0^2=4$ GeV^2, which give the overall optimum fit, are

$$\begin{aligned} x[u_v(x)+d_v(x)] &= 0.38x^{0.27}(1-x)^{3.93} \\ &\quad \times(1+9.9x^{1/2}+17.7x) , \\ x\,d_v(x) &= 1.50x^{0.61}(1-x)^{4.68}(1+1.08x^{1/2}) . \end{aligned} \tag{40}$$

The small-x behavior of these valence distributions is tightly constrained by the behavior of the ratio $F_2^{\mu n}/F_2^{\mu p}$ which is now measured very precisely by the NMC.[27] The exponent of x for $x(u_v+d_v)$ may seem low when compared with the naive Regge expectation of $\frac{1}{2}$ but the measured convergence of the Gottfried sum rule is quite consistent with this value.

In order to gauge the sensitivity to measurements in the small-x region, we also perform a fit with a traditional-type gluon satisfying $xg(x,Q_0^2)\to$const as $x\to 0$. This fit is labeled B_0 and also uses $\Lambda_{\overline{\rm MS}}^{(n_f=4)}=0.19$ GeV but the parton distributions at $Q_0^2=4$ GeV^2 are found to be

$$\begin{aligned} xg(x) &= 2.87(1-x)^{5.1} , \\ xS(x) &= 0.55(1-x)^{10}(1+6.1x^{1/2}+4.2x) , \\ x[u_v(x)+d_v(x)] &= 0.42x^{0.27}(1-x)^{3.92} \\ &\quad \times(1+8.1x^{1/2}+17.3x) , \\ xd_v(x) &= 1.49x^{0.61}(1-x)^{4.67}(1+1.12x^{1/2}) . \end{aligned} \tag{41}$$

Before going on to study the small-x region which is yet unexplored we demonstrate that the above fits are indeed consistent with existing data. As an example we show in Fig. 6 the comparison with $F_2^{\mu p}$ data from BCDMS and in Fig. 7 the comparison with the $F_2^{\mu n}/F_2^{\mu p}$ ratios measured by NMC, BCDMS, and EMC. The preliminary data from NMC have very small uncertainties and significantly constrain the parameters which govern the small-x region. The quality of the fits to the data for the various processes is illustrated in Table I, together with the corresponding χ^2 values of our previous HMRS(B) set of partons.[9]

Next we inspect how low in x we can get experimental constraints from existing F_2 data without going below

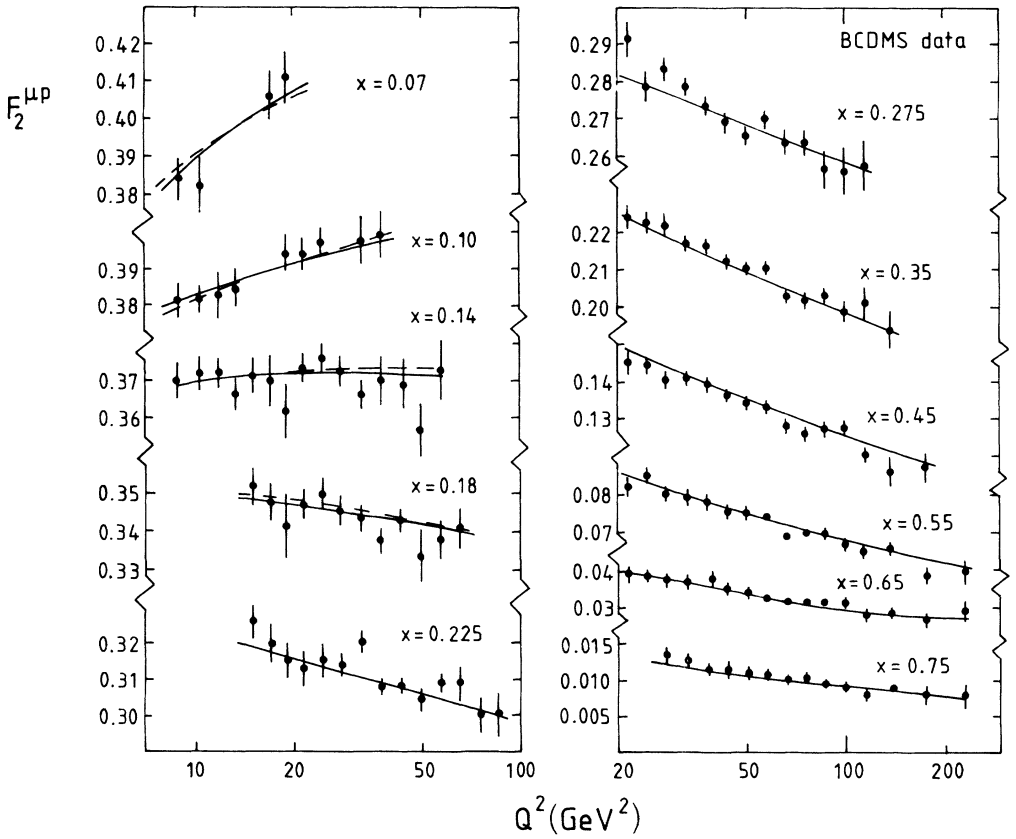

FIG. 6. $F_2^{\mu p}(x,Q^2)$ from BCDMS (Ref. 5) renormalized down by 2%. The curves correspond to the two fits B_- and B_0 described in the text. For those x values where the two fits are distinguishable, B_- is shown as a solid line, B_0 as a dashed line.

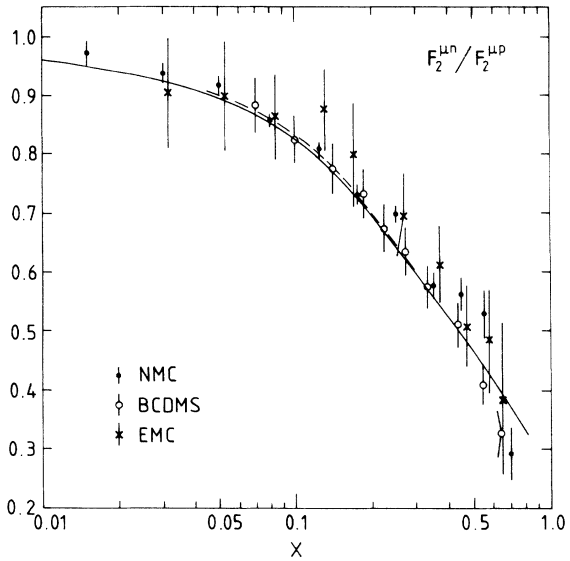

FIG. 7. The measurements of $F_2^{\mu n}/F_2^{\mu p}$ by EMC (Ref. 25), BCDMS (Ref. 26), and NMC (preliminary) (Ref. 27). The values of Q^2 vary across the x range and the calculated values take this into account. Where the curves of the two fits are distinguishable, B_- is shown as a solid line, B_0 as a dashed line.

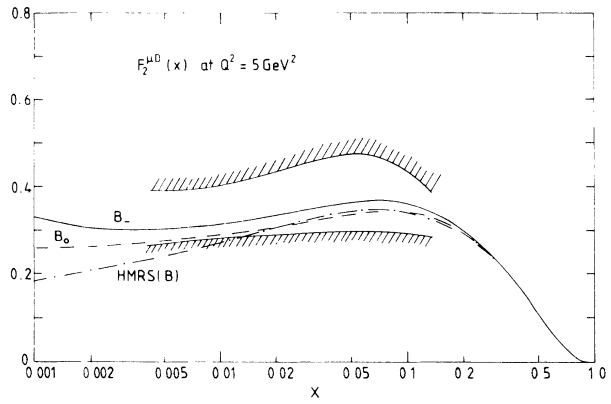

FIG. 8. $F_2^{\mu D}(x)$ at $Q^2=5$ GeV^2. The shaded lines represent realistic upper and lower experimental limits obtained from the recent EMC data (Ref. 3), together with previous data. The predictions obtained from the B_- and B_0 sets of partons are shown as solid and dashed curves, respectively. Also indicated is the prediction of the HMRS(B) partons of Ref. 9.

our Q^2 cutoff of 4 GeV^2. Recent deep-inelastic data from EMC[3] on deuterium have probed down to $x=0.0015$; however, the Q^2 values there are below 2 GeV^2. If we fix $Q^2=5$ GeV^2 then we can get realistic limits on $F_2^{\mu D}$ down to $x=0.004$. Figure 8 shows our estimates for these experimental limits, together with the predictions of $F_2^{\mu D}$ obtained from the B_- and B_0 sets of partons. It is clear that the data do not suggest any rise at low x as one might naively expect from a $x^{-1/2}$ behavior of the sea and gluon. We can see that our B_- prediction only begins to grow around $x=10^{-3}$. For comparison we also show the HMRS(B) fit of Ref. 9 where the parametrization at $Q_0^2=4$ GeV^2 allowed the sea to actually vanish at $x=0$. As we evolve to higher Q^2 this zero of course disappears, but we can see from Fig. 8 that this type of small-x behavior is disfavored by the experimental bounds, as well as being suspect theoretically. As Q^2 increases, the evolution of the sea produces the familiar rise at small x even for the B_0 fit. Figure 9 shows the behavior of the proton structure function at $Q^2=20$ GeV^2 predicted at small x, together with the quality of the fit to the data available at larger x. We see that between x of 10^{-2} to 10^{-1} the shape is essentially flat but below 10^{-2} the $x^{-1/2}$ behavior associated with the B_- fit results in a more dramatic increase.

Now we turn to the effects of shadowing discussed in Sec. III to see what modifications to the $x^{-1/2}$ behavior of the gluon and sea distributions could be discernible at low x. Since the role of shadowing is to restore consistency of the "semihard" cross sections with the Froissart bound, it is expected to give the largest modifications to our B_- set of parton distributions. An approximate general form of the shadowing corrections to the gluon "starting" distribution was given in (33). In the expression for $xg_{\mathrm{sat}}(x)$ given in (34) we consider two values of the radius $R=5$ GeV^{-1} and 2 GeV^{-1} representing the two distinct limits: (i) gluon ladders coupling to different partons and (ii) gluon ladders coupling to the same parton. Figure 10 shows that at $Q_0^2=4$ GeV^2 there is a difference at $x=10^{-3}$ between the unshadowed gluon and

TABLE I. The contributions to χ^2 resulting from the various fits to the data. Note that the preliminary NMC data (Ref. 27) were slightly different for the HMRS analysis (Ref. 9) although the entry in the table corresponds to the current values. Prompt photon data of WA70 (Ref. 28) were also used to constrain the parton distributions.

Data	No. points	χ^2 values B_-	B_0	HMRS(B)
$F_2^{\mu p}$ (BCDMS, Ref. 5)	142	134	140	164
$F_2^{\nu N}$ (CDHSW, Ref. 6)	84	77	57	55
$xF_3^{\nu N}$ (CDHSW, Ref. 6)	94	61	60	115
$F_2^{\mu n}/F_2^{\mu p}$ (BCDMS, Ref. 26)	11	5	5	9
$F_2^{\mu n}/F_2^{\mu p}$ (EMC, Ref. 25)	10	4	3	3
$F_2^{\mu n}/F_2^{\mu p}$ (NMC, Ref. 27)	11	27	22	15
Drell-Yan (E605, Ref. 29)	8	16	16	12

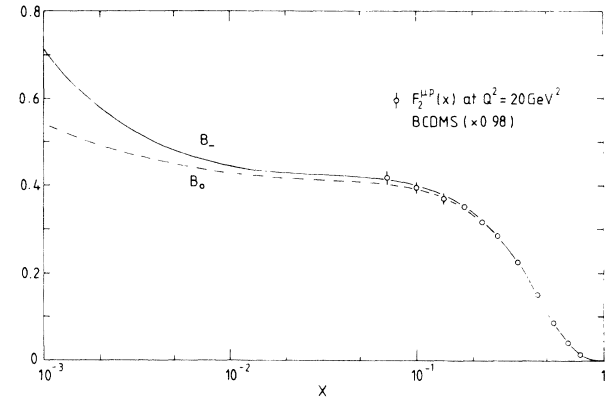

FIG. 9. $F_2^{\mu p}(x)$ at $Q^2=20$ GeV^2 showing the quality of the fits to the BCDMS data (Ref. 5) and the predictions for small x. The effect of shadowing is shown in Fig. 12.

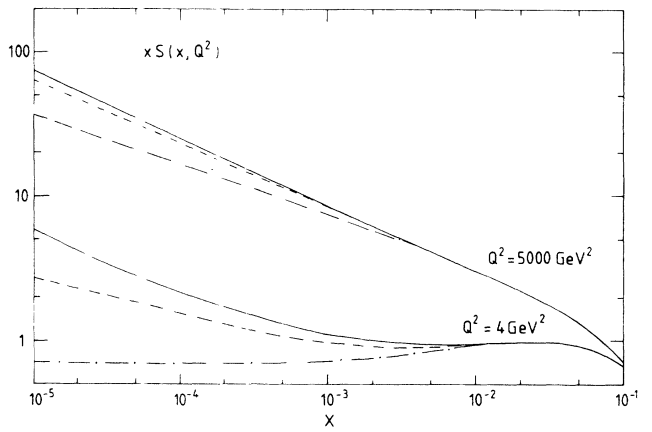

FIG. 11. The sea-quark distribution $xS(x,Q^2)$ at $Q^2=Q_0^2$ and 5000 GeV^2. The lines are labeled as in Fig. 10.

the "partonic"-type shadowed gluon of nearly 30%. As x decreases further, the separation between the unshadowed and the two shadowed gluons becomes substantial of course. As the gluon is evolved to higher Q^2, this separation is less dramatic and Fig. 10 also shows the resulting gluons at $Q^2 \simeq M_W^2$ where there is no difference at $x=10^{-3}$ any more.

We also include the shadowing corrections to the sea-quark distributions. First we modify the "starting" distribution at $Q^2=Q_0^2=4$ GeV^2 at small x, as in (35). The result is shown in Fig. 11. Then we modify the evolution equation for the sea quarks by including the two additional shadowing contributions given in (36). Figure 11 also shows the sea-quark distribution at high Q^2 where now the relative effect of shadowing is similar to that for gluons at the same Q^2, as we expect. In Sec. VI we investigate if experiments at HERA will be able to reveal the presence of the shadowing corrections.

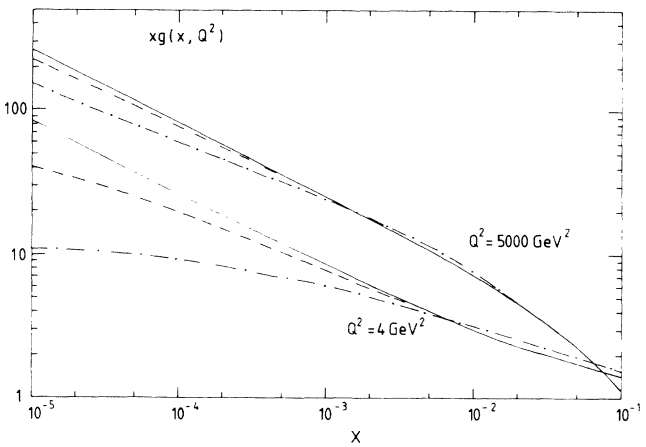

FIG. 10. The gluon distribution $xg(x,Q^2)$ at $Q^2=Q_0^2=4$ GeV^2 and $Q^2=5000$ GeV^2. The unshadowed gluon from the B_- fit is shown as a solid line, shadowing with $R=5$ GeV^{-1} as a dashed line, and shadowing with $R=2$ GeV^{-1} as a dot-dashed line. The differences for $x>0.01$ result from adjusting the normalization of the shadowed gluon to carry the same fraction of momentum.

The shadowing contributions to the gluon and sea-quark evolution equations were also included for the B_0 set of partons. They are found to make much less difference and for simplicity we do not show B_0 predictions with shadowing effects. It is interesting to note that the B_- sea-quark distribution maximally corrected for shadowing (i.e., $R=2$ GeV^{-1}) is similar to that of B_0, and hence the predictions for F_2^{ep} will also be similar (see Sec. VI). The gluon distributions, on the other hand, are still significantly different at very small x, and this difference is manifested in the predictions for the longitudinal structure function F_L (see Sec. VI). The conventional belief, however, is that the B_- distributions with the more modest shadowing corrections ($R\sim 5$ GeV^{-1}) will give the more reliable predictions. In this case the sea quarks and the gluons are dramatically different from those of the B_0 set.

Let us look in more detail at the B_- set of partons. Could we have anticipated the magnitude of the sea distribution at small x from the gluon? At first sight it appears that the size of the sea at small x (controlled by $A_s=0.0168$) is very small compared to that of the gluon ($A_g=0.265$). However, as we shall see in the next section, the magnitude of A_s/A_g is in good agreement with our theoretical expectations.

V. CONSISTENCY CHECKS FOR THE GLUON-SEA RATIO AT SMALL x

There is an intimate connection between the gluon and the sea-quark distributions. Indeed it is interesting to check whether the theoretical estimates for the sea-to-gluon ratio

$$\frac{xS(x,Q_0^2)}{xg(x,Q_0^2)} \sim \frac{A_s}{A_g} \tag{42}$$

at small x are consistent with the ratio of the values of the parameters A_s and A_g found in the B_- fit to the data presented in Sec. IV, namely,

$$\frac{A_s}{A_g}=\frac{0.0168}{0.265}=0.063\ . \tag{43}$$

When shadowing is neglected, the leading $x^{-1/2}$ behavior of xg and xS is unchanged by the QCD evolution (see Sec. II), and the Q^2 dependence at small x lies in the coefficients; that is, we may take $A_s \to A_s(Q^2)$ and $A_g \to A_g(Q^2)$. If we assume that $A_s(\tilde{Q}_0^2)=0$ at some low scale $\tilde{Q}_0^2$ then we can compute the ratio $A_s(Q^2)/A_g(Q^2)$ in terms of the evolution length parameter

$$\tilde{\xi}(Q^2)=\int_{\tilde{Q}_0^2}^{Q^2}\frac{dq^2}{q^2}\frac{C_A\alpha_s(q^2)}{\pi}\ , \tag{44}$$

which is defined in analogy to (5). The relevant LL(Q^2) formulas for $A_s(Q^2)$ and $A_g(Q^2)$ are (B.9) and (B.10) of Ref. 31. We find that we can reproduce the numerical ratio (43) provided that we take $\tilde{Q}_0^2=1.3\ \mathrm{GeV}^2$. In fact this theoretical estimate always gives $A_s(Q_0^2)/A_g(Q_0^2)<0.18$ and only reaches the upper bound when $\tilde{Q}_0^2\to\Lambda^2$, i.e., $\tilde{\xi}(Q_0^2)\to\infty$.

A second consistency check is provided by estimating the sea-quark distribution $xS_{\mathrm{sat}}(x,Q^2)$ from the saturation limit of the gluon distribution, $xg_{\mathrm{sat}}(x,Q^2)$ of (34). We have, keeping only the LL(Q^2) $g\to q\bar{q}$ transition,

$$xS_{\mathrm{sat}}(x,Q^2)\simeq\tfrac{2}{3}N_f\int^{Q^2}\frac{dq^2}{q^2}\frac{\alpha_s(q^2)}{2\pi}xg_{\mathrm{sat}}(x,q^2)$$
$$\sim\frac{\alpha_s(Q^2)}{\pi}xg_{\mathrm{sat}}(x,Q^2)\ , \tag{45}$$

where the $\frac{2}{3}$ arises from the x integration, and where we have used the Q^2 dependence of (34) to evaluate the integral and set $N_f=3$. Of course, in general, the relation between the saturation limits is more complicated,[32] but (45) should be more than adequate for the estimate that we require. From (45) we have

$$\frac{xS_{\mathrm{sat}}(x,Q_0^2)}{xg_{\mathrm{sat}}(x,Q_0^2)}\sim\frac{\alpha_s(Q_0^2)}{\pi}\sim0.08\ . \tag{46}$$

When this is combined with

$$\frac{xS_{\mathrm{sat}}(x,Q_0^2)}{xg_{\mathrm{sat}}(x,Q_0^2)}=\frac{A_s}{A_g}\ ,$$

which follows from (35), the resulting theoretical estimate for A_s/A_g is again seen to be in excellent agreement with the ratio (43) obtained from the phenomenological analysis.

VI. EXPERIMENTS AT HERA, LHC, AND SSC AS A PROBE OF SMALL x

The first definitive test of the small-x behavior of the parton distributions discussed in the preceding sections will come from the HERA ep collider. Detailed studies[33] have shown that, operating at the standard center-of-mass energy $\sqrt{s}=314$ GeV, the F_2^{ep} structure function can be measured in the kinematic region of x and Q^2 defined by

$$x/Q^2\gtrsim10^{-5}\ \mathrm{GeV}^{-2}\ . \tag{47}$$

Note that since we are here interested primarily in the small-x region, we can neglect the contribution to F_2 from Z exchange.

In a previous study,[9] we examined the predictions for F_2 in the moderate x, large-Q^2 region. We showed that differences in F_2 at currently accessible Q^2 values [$<0(100\ \mathrm{GeV}^2)$] as parametrized, for example, by the HMRS(E) and HMRS(B) distributions, persist to the higher Q^2 values relevant to HERA.[9] Different $\Lambda_{\overline{\mathrm{MS}}}$ values can also cause the predictions to diverge slightly at higher Q^2.[9]

Turning to the small-x region, Fig. 12 shows the predictions for the structure function F_2^{ep} for the different sets of partons down to $x=10^{-4}$ at the representative value of $Q^2=20\ \mathrm{GeV}^2$. The curves correspond to the B_- and B_0 predictions, with strong ($R=2\ \mathrm{GeV}^{-1}$) and weak ($R=5\ \mathrm{GeV}^{-1}$) shadowing included for B_-. We see that it will be difficult to establish the existence of shadowing effects for $x>10^{-3}$. Even the extreme form of the shadowing correction only reduces F_2^{ep} by about 10% at $x=10^{-3}$.

We can regard Fig. 12 as giving a reasonable representation of the spread in predictions for F_2^{ep} at HERA. All the sets of partons are completely compatible with existing deep-inelastic data and it is difficult to select a "best" prediction. As explained in previous sections the different curves represent different choices of theoretical input. The most physically reasonable expectation is probably the prediction for B_- corrected for shadowing with $R=5\ \mathrm{GeV}^{-1}$. The prediction with $R=2\ \mathrm{GeV}^{-1}$ shadowing can be then taken as an extreme lower bound and the unshadowed B_- prediction as an upper bound. We argued in Sec. II that the B_0 set of partons is disfavored theoretically but we see from Fig. 12 that it will

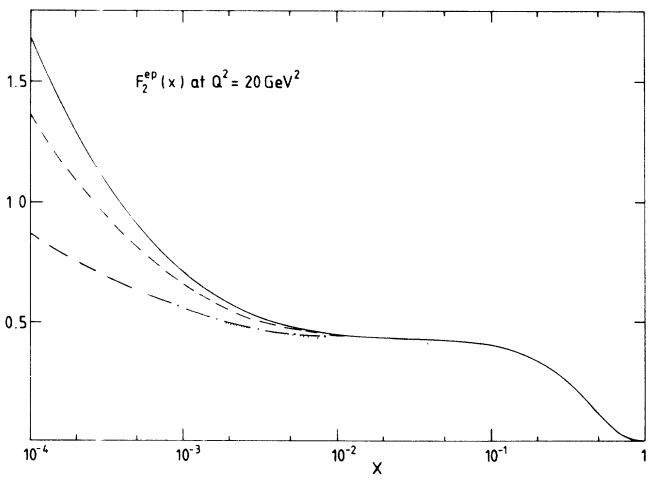

FIG. 12. The structure function F_2^{ep} ($=F_2^{\mu p}$) as a function of x at $Q^2=20\ \mathrm{GeV}^2$. The solid line is the continuation of the B_- fit (Fig. 9) down to $x=10^{-4}$. The dashed and dot-dashed lines indicate the correction due to shadowing with $R=5$ and 2 GeV^{-1}, respectively. For comparison the prediction from the B_0 set of partons is shown by the dotted curve.

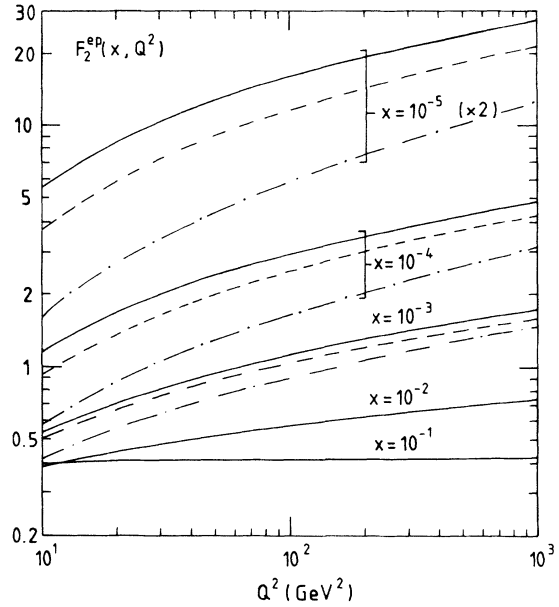

FIG. 13. $F_2^{ep}(x,Q^2)=F_2^{\mu p}(x,Q^2)$ for $10^{-5}\leq x\leq 10^{-1}$ and $10<Q^2<1000$ GeV^2. The upper, middle, lower lines correspond to the B_- fit, unshadowed and shadowed with $R=5$ GeV^{-1}, 2 GeV^{-1}, respectively.

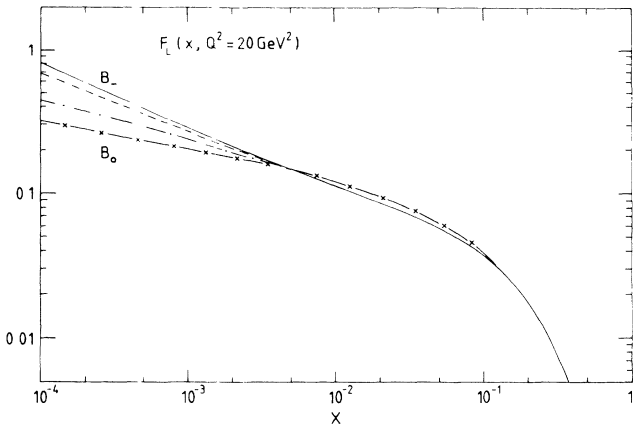

FIG. 14. The longitudinal structure function $F_L(x,Q^2)$ as a function of x at $Q^2=20$ GeV^2. The solid, dashed, and dot-dashed lines show the predictions for the B_- set of partons with no shadowing, shadowing with $R=5$ GeV^{-1} and $R=2$ GeV^{-1}, respectively. The line with crosses is the result for the B_0 fit.

be difficult to distinguish this solution from the B_- set, maximally corrected for shadowing ($R=2$ GeV^{-1}), by measurements of F_2^{ep} at HERA.

For completeness the predictions for F_2^{ep} using shadowed and unshadowed partons are shown in Fig. 13 over a wide range of x and Q^2. The differences at very small x are dramatic, and measurements of F_2^{ep} there would of course be much more revealing. For example, an electron-proton collider in the CERN LEP tunnel with $\sqrt{s}=2(0.05\ \text{TeV}\times 8\ \text{TeV})^{1/2}=1.3$ TeV and with a luminosity of order 10^{32} cm^{-2} would be capable of measuring F_2^{ep} down to $x\sim 10^{-6}$ at $Q^2\sim 10$ GeV^2.[34]

The longitudinal structure function F_L will also be measured at HERA. We have already shown[30] how, in perturbative QCD, F_L is a sensitive probe of the gluon distribution. In fact to $O(\alpha_s)$ we have, to a good approximation at small x, the direct relation[35]

$$xg(x,Q^2)\simeq 1.77\frac{3\pi}{2\alpha_s(Q^2)}F_L(0.4x,Q^2)\ , \tag{48}$$

where we have omitted a small contribution from F_2; that is, the gluon distribution can be simply read off the measurements of F_L by rescaling the x value by 0.4. From Fig. 14 we see that an accurate measurement of F_L below $x\simeq 10^{-3}$ will provide a way of distinguishing the nature of the small-x gluon. Notice that even the "maximally" shadowed $x^{-1/2}$-type gluon leads to a softer $F_L(x)$ than the traditional "constant"-type gluon. Because of the $\alpha_s(Q^2)$ in (48) the variation of $F_L(x,Q^2)$ with Q^2 is not rapid; going from $Q^2=20$ up to 200 GeV^2 makes a difference of 10% or less.

The production of relatively light final states in very-high-energy hadron-hadron collisions also provides a way to probe the small-x behavior of the parton distributions. In Ref. 20 we studied the production of heavy-quark pairs and Higgs bosons by gluon-gluon fusion. The cross sections do exhibit the expected sensitivity to the gluon distribution; for example, $\sigma(b\bar{b})$ probes the gluon for $x\gtrsim 2m_b/\sqrt{s}$. However, it is not clear that such cross sections could be reconstructed experimentally with sufficient accuracy to allow a definite determination.

Another process which is, in principle, capable of exploring the very-small-x behavior of quark distributions is weak-boson production in proton-proton collisions. It was pointed out in Ref. 36 that a significant contribution to the W and Z production cross sections at energies of the CERN Large Hadron Collider (LHC) (16 TeV) and the Superconducting Super Collider (SSC) (40 TeV) energies comes from the annihilation of a relatively-large-x valence quark with a very-small-x sea quark. We would expect, therefore, that the predictions for σ_W and σ_Z at these energies using the B_- and B_0 distributions would be very different. This is illustrated in Fig. 15. The predictions for the HMRS(B) partons[9] are, as expected, very similar to the B_0 predictions shown in Fig. 15; to be precise they lie 2% below the B_0 values at present $p\bar{p}$ collider energies and 5% below at SSC energies. Note that the agreement of all sets [i.e., B_0,B_-, HMRS(B), as well as E_-, HMRS(E) shown in Ref. 30] with the W and Z cross section measurements from UA2 (Ref. 37) and CDF (Ref. 38) is very good. This is not surprising since at the $p\bar{p}$ collider energies the distributions are being sampled at x values where there are constraints from deep-inelastic data, albeit at lower Q^2. However, a measurement uncertainty of order 20% or less at LHC and SSC energies would be more than sufficient to confirm the singular B_- type partons (with reasonable shadowing) as opposed to the traditional B_0 set of partons. The spread of uncertainty in the theoretical predictions will only be reduced when measurements of F_2^{ep} at small x become available from HERA. Because of the asymmetry in the momen-

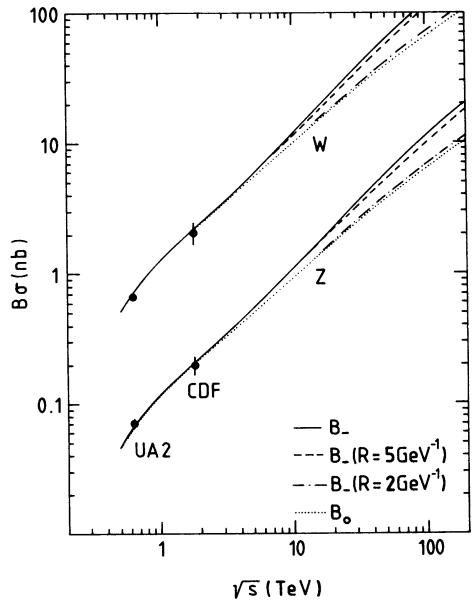

FIG. 15. The W and Z cross sections as a function of the $p\bar{p}$ collider energy, as calculated using the B_- (solid curves) and B_0 (dotted curves) sets of partons. The dashed and dot-dashed curves correspond to the B_- predictions with shadowing corrections with $R=5$ and 2 GeV^{-1}, respectively. The data points correspond to the measurements of the UA2 (Ref. 37) and CDF (Ref. 38) Collaborations. At LHC and SSC energies $\sigma_{W,Z}(pp)=\sigma_{W,Z}(p\bar{p})$ to within less than 1%.

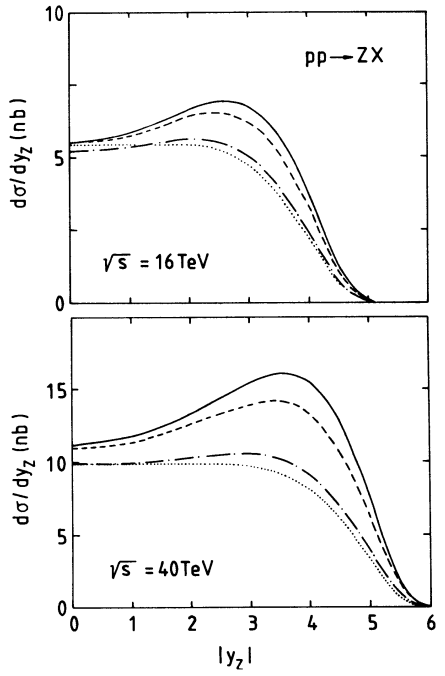

FIG. 16. The rapidity distribution of Z bosons produced in pp collisions at $\sqrt{s}=16$ TeV and $\sqrt{s}=40$ TeV as predicted by the B_- and B_0 sets of partons. The unshadowed B_- prediction is shown as a solid line, shadowing with $R=5$ GeV^{-1} as a dashed line, and shadowing with $R=2$ GeV^{-1} as a dot-dashed line. The dotted line is the B_0 prediction. The details of observing the produced Z by its $\mu^+\mu^-$ decay mode are discussed in Ref. 36.

tum fractions of the colliding quark and antiquark, a substantial fraction of the W and Z bosons is produced at large rapidity. The steeper the sea-quark distributions at very small x, the larger the fraction. Thus Fig. 16 shows the Z rapidity distributions at LHC and SSC energies, for all the B_- sets as well as B_0. Note the qualitatively different behavior at large y. A similar effect was found in Ref. 36, where the E_+, E_-, and HMRS(E) distributions were used.

VII. CONCLUSIONS

In our view the most interesting physics that will be revealed by the forthcoming experiments at HERA will be new phenomena at small x ($\lesssim 10^{-2}$). For the first time we attempt to incorporate the theoretical QCD behavior expected in this unexplored small-x regime into a phenomenological description of quark and gluon distributions which are consistent with data in the x region already probed by experiment. To be precise we have performed a detailed next-to-leading-order QCD analysis of all the relevant data in order to extract a definitive set of parton distributions $f_i(x,Q^2)$ that may be reliably extrapolated to very small x. The parametric forms of the "starting" distributions $xf_i(x,Q^2=4\ \text{GeV}^2)$ were chosen to incorporate the theoretically motivated $x^{-1/2}$ behavior of the gluon and the sea-quark distributions at small x, so that we are able to make realistic predictions for very-small-x values, i.e., for x in the range $10^{-5}\lesssim x\leq 10^{-2}$, much below the x values of the existing data. Only part of this range will be probed by HERA; nevertheless, the parton distributions are required throughout this range in order to make realistic predictions for physics at LHC and SSC energies.

Given the above $x^{-1/2}$ behavior, shadowing corrections are found to be increasingly important as x decreases through the above interval. The shadowing effects enter both the gluon and the sea-quark distributions at small x through (i) modifications of the "starting" distributions and (ii) the presence of additional nonlinear terms in the Q^2-evolution equations. The shadowing corrections arise from the need to tame the rapid growth of gluons at very small x ($x\lesssim 10^{-3}$) so that the unitarity limit is respected. We speak of gluon saturation. Through $g\to q\bar{q}$ splitting, and related effects, there is a comparable slowing down of the Q^2 evolution of the sea-quark distributions at very small x. We find that the shadowing corrections to the gluon and sea quarks lead to significant modifications to the predictions for the behavior of the structure functions F_L and F_2, respectively, in the small-x, moderate Q^2, range accessible to experiments at HERA. Moreover, we note that the observation of Z production at large rapidity at LHC and SSC energies can probe the behavior of sea quarks at ultrasmall x ($x\lesssim 10^{-4}$).

There are several attractive features of the present analysis. First we are able to describe a wide range of data for different processes in terms of a relatively small number of parameters. Moreover, the parametric forms are prescribed by underlying QCD theory. It is also satisfying to note that the values of the parameters describing

the small-x behavior of the gluon and sea-quark distributions come out to be very much as expected. Finally, a very important feature of the analysis is that different versions of shadowing can, in principle, be distinguished by experiment. We have considered two extreme possibilities corresponding to radically different ways in which the gluons are concentrated in the proton: (i) distributed uniformly across the proton or (ii) localized in "hot spots" associated with a single valence quark. However, we should note that a slight variation of the unshadowed $x^{-\lambda}$ behavior, away from the canonical choice of $\lambda=0.5$, will give a residual uncertainty in the precise extraction of the shadowing contribution. In the future it may be possible to solve the Lipatov equation more precisely, so reducing this uncertainty, and hence to isolate shadowing effects more directly from data at very low x.

In summary, we have extracted from high-statistics experimental data (for $x>0.01$) parton distributions which incorporate the expected singular behavior *and* the shadowing corrections at very small x. The conventional expectation for shadowing is nearer (i) than (ii), as defined above, corresponding to the B_- set of partons with $R\sim 5$ GeV^{-1}, but we eagerly await the measurements of the forthcoming low-x experiments.

The four sets of parton distributions described in this work can be obtained by electronic mail from WJS@UK.AC.DUR.HEP.

ACKNOWLEDGMENTS

We thank Peter Harriman for useful discussions and one of us (J.K.) thanks the U. K. Science and Engineering Research Council and the University of Durham for financial support. J.K. would also like to thank the Physics Department and Grey College of the University of Durham for very warm hospitality.

*On leave from the H. Niewodniczanski Institute of Nuclear Physics, 31-342 Krakow, Poland.

[1]L. V. Gribov, E. M. Levin, and M. G. Ryskin, Phys. Rep. **100**, 1 (1982).

[2]T. K. Gaisser and F. Halzen, Phys. Rev. Lett. **54**, 1754 (1985); G. Pancheri and Y. N. Srivastava, Phys. Lett. B **182**, 199 (1986); L. Durand and H. Pi, Phys. Rev. Lett. **58**, 303 (1987); Phys. Rev. D **40**, 1436 (1989); J. Kwiecinski, Phys. Lett. B **184**, 386 (1987).

[3]European Muon Collaboration (EMC), M. Arneodo *et al.*, Nucl. Phys. **B333**, 1 (1990).

[4]European Muon Collaboration (EMC), J. J. Aubert *et al.*, Nucl Phys. **B259**, 189 (1985).

[5]Bologna-CERN-Dubna-Munich-Saclay (BCDMS) Collaboration, A. C. Benvenuti *et al.*, Phys. Lett. B **223**, 485 (1989).

[6]CERN-Dortmund-Heidelberg-Saclay-Warsaw (CDHSW) Collaboration, J. P. Berge *et al.*, CERN Report No. CERN-EP/89-103, 1989 (unpublished).

[7]Chicago-Columbia-Fermilab-Rochester-Rockefeller (CCFRR) Collaboration, E. Oltman, Columbia University thesis, Nevis Report No. 270.

[8]A. H. Mueller and J. Qiu, Nucl. Phys. **B268**, 427 (1986).

[9]P. N. Harriman, A. D. Martin, W. J. Stirling, and R. G. Roberts, Phys. Rev. D **42**, 798 (1990) (HMRS).

[10]A. De Rújula *et al.*, Phys. Rev. D **10**, 1649 (1974); Yu. L. Dokshitzer, D. I. Dyakonov, and S. I. Troyan, Phys. Rep. **58C**, 269 (1980).

[11]Ya. Ya. Balitzkij and L. N. Lipatov, Yad. Fiz. **28**, 1597 (1978) [Sov. J. Nucl. Phys. **28**, 822 (1978)]; J. B. Bronzan and R. L. Sugar, Phys. Rev. D **17**, 585 (1978); L. N. Lipatov, Zh. Eksp. Teor. Fiz. **90**, 1536 (1986) [Sov. Phys. JETP **63**, 904 (1986)]; T. Jaroszewicz, Acta Phys. Pol. B **11**, 965 (1980); L. N. Lipatov, in *Perturbative QCD,* edited by A. H. Mueller (World Scientific, Singapore, 1989), p. 411.

[12]J. C. Collins and J. Kwiecinski, Nucl. Phys. **B316**, 307 (1989).

[13]L. V. Gribov, E. M. Levin, and M. G. Ryskin, Nucl. Phys. **B188**, 155 (1981).

[14]L. V. Gribov, E. M. Levin, and M. G. Ryskin, Zh. Eksp. Teor. Fiz. **80**, 2132 (1981) [Sov. Phys. JETP **53**, 1113 (1981)].

[15]R. J. Glauber, in *Lectures in Theoretical Physics,* edited by W. E. Brittin and L. G. Dunham (Interscience, New York, 1959), Vol. 1, p. 315.

[16]E. M. Levin and M. G. Ryskin, Phys. Rep. **189**, 267 (1990).

[17]E. M. Levin, in *Proceedings of the Topical Workshop on the Small-x Behavior of Deep Inelastic Scattering Structure Functions in QCD,* Hamburg, Germany, 1990, edited by A. Ali and J. Bartels [Nucl. Phys. B (Proc. Suppl.) (in press)].

[18]M. G. Ryskin, in *Weak Interactions and Neutrinos,* proceedings of the Twelfth International Workshop, Ginosar, Israel, 1989, edited by P. Singer and B. Gad Eilam [Nucl. Phys. B (Proc. Suppl.) **13**, 40 (1990)].

[19]J. Kwiecinski, Z. Phys. C **29**, 147 (1985).

[20]J. C. Collins and J. Kwiecinski, Nucl. Phys. **B335**, 89 (1990).

[21]A. H. Mueller, Nucl. Phys. **B335**, 119 (1990); A. H. Mueller, in *Proceedings of the Topical Workshop on the Small-x Behavior of Deep Inelastic Scattering Structure Functions in QCD,* edited by A. Ali and J. Bartels (Ref. 17).

[22]M. Glück, E. Reya, and A. Vogt, Dortmund University Report No. DO-TH 89/20 (unpublished).

[23]A. D. Martin, R. G. Roberts, and W. J. Stirling, Phys. Rev. D **37**, 1161 (1988); Phys. Lett. B **206**, 327 (1988); Mod. Phys. Lett. A **4**, 1135 (1989).

[24]L. W. Whitlow *et al.*, SLAC Report No. SLAC-PUB-5100, 1989 (unpublished).

[25]European Muon Collaboration (EMC), J. J. Aubert *et al.*, Nucl. Phys. **B293**, 740 (1987).

[26]Bologna-CERN-Dubna-Munich-Saclay (BCDMS) Collaboration, A. C. Benvenuti *et al.*, Phys. Lett. B **237**, 599 (1990).

[27]New Muon Collaboration (NMC), presented by C. Peroni at the Workshop on Hadron Structure Functions, Fermilab, Batavia, Illinois, 1990 (unpublished).

[28]WA70 Collaboration, M. Bonesini *et al.*, Z. Phys. C **38**, 371 (1988).

[29]E605 Collaboration, C. N. Brown *et al.*, Phys. Rev. Lett. **63**, 2637 (1989).

[30]P. N. Harriman, A. D. Martin, W. J. Stirling, and R. G. Roberts, Phys. Lett. B **243**, 421 (1990).

[31]J. Kwiecinski and D. Strozik-Kotlorz, Z. Phys. C (to be published).

[32]E. M. Levin and M. G. Ryskin, Frascati INFN report, 1990 (unpublished); see also Ref. 17.

[33]Proceedings of the HERA Workshop, DESY, 1988, edited by

R. D. Peccei (unpublished).
[34]J. Feltesse, presented at the European Committee for Future Accelerators (ECFA) Workshop on Physics at the LHC Collider, CERN, Geneva, Switzerland, 1990 (unpublished).
[35]A. M. Cooper-Sarkar *et al.*, Z. Phys. C **39**, 281 (1988).
[36]A. D. Martin and W. J. Stirling, Phys. Lett. B **248**, 443 (1990).
[37]UA2 Collaboration, J. Alitti *et al.*, Z. Phys. C **47**, 11 (1990).
[38]CDF Collaboration, presented by P. Derwent at the XXV Rencontre de Moriond, 1990 (unpublished).